Poster2-09 SPATIAL-TEMPORAL EVOLUTIONS OF PRECIPITATION CORES AND LIGHTNING ACTIVITY OBSERVED BY PHASED ARRAY WEATHER RADARS AND BOLT

Yukie Moroda [12], Kazuhisa Tsuboki [2], Shinsuke Satoh [1], Katsuhiro Nakagawa [1],
Tomoo Ushio [3], Hiroshi Kikuchi [4]
[1]National Institute of Information and Communications Technology, Koganei, Japan
[2]Institute for Space-Earth Environment Research, Nagoya University, Nagoya, Japan
[3]Department of Aerospace Engineering, Tokyo Metropolitan University, Hino, Japan
[4]University of Electro-Communications, Tokyo, Japan

1. INTRODUCTION

Many cumulonimbus clouds develop and cause lightning during summer season in Japan. A cumulonimbus cloud is considered to be composed of a precipitation cell. A large reflectivity region in the precipitation cell which contains a large amount of precipitation particles such as graupel is defined as a precipitation core. The noninductive charging mechanism with graupel particles plays an important role in lightning formation (Takahashi 1978). Many previous studies have shown that the height of large reflectivity region corresponds to that of a intracloud lightning occurrence height and flash rate (eg., Emersic et al., 2011; Yoshida et al., 2016). However, the relationship between evolution of precipitation core and lightning activity is still not clarified. Three dimensional structure of precipitation core corresponds to localized heavy rain (Shusse et al., 2015). Therefore, detailed information about three dimensional structure of precipitation core is useful to find an onset of a localized heavy rain. Understanding the relationship clarifies how a lightning activity is related to a localized heavy rain. It is, however, difficult to investigate the rapid temporal variation of the three dimensional structure of precipitation core using conventional weather radar. Recently, phased array weather radars (PAWRs) enable us to identify precipitation cores with a high resolution spatial-temporal observation. In this study, we examine evolution of three dimensional structure of precipitation core and lightning activity every 30 sec. Our goal is to clarify the spatial-temporal relationship between precipitation core and lightning activity.

2. DATA AND METHODS

Two X-band PAWRs are located at Suita City, Osaka Prefecture and Kobe City, Hyogo Prefecture, and thirteen sensors of Broadband Observation network for Lightning and Thunderstorm (BOLT: Yoshida et al., 2014) located in Osaka and Hyogo Prefectures (Fig. 1). PAWRs observe 360 degrees in azimuth with an azimuthal resolution of 1.2 degree and 90 degrees in elevation with 1 degree within 30 seconds. The observation range of PAWRs is 60 km with a range resolution of 100 m. PAWRs reflectivity data were converted from polar to Cartesian coordinates (Cressman 1959). The horizontal and vertical resolutions are 250 m, respectively. We employed the larger reflectivity value in the same grid obtain from the two PAWRs observations.

BOLT is a sensor network to detect the LF-band electromagnetic wave, and observe source points of intracloud (IC) and cloud-to-ground (CG) discharges in the three dimensions. A pulse peak is observed by each sensor, and then the positions are identified in 80 μs time window. Three-dimensional source points are estimated by time of arrival technique based on Yoshida et al. (2014). Errors of horizontal and vertical directions are less than 100 m and 400 m, respectively. Source points were grouped into a flash within the range and time interval of 20 km and 150 ms, respectively. We identify 10 or more BOLT sources as a flash. To eliminate noise signals, we check a BOLT source, which employed initiation point in a flash, closed to following BOLT sources. CG flashes are defined as a flash contains more than 10 BOLT sources below 1.0 km in height.

4. RESULTS

The thunderstorm was observed during the period from 1600 to 1800 LST on 7 August 2015 in the analysis area (Fig. 1). Three dimensional continuous echo region larger than 55 dBZ is defined as a precipitation core. To focus clear precipitation cores, we identify the precipitation cores that the volume was larger than 1 km^3 and the volume and intensify were maintained longer than 3 min. The cell was composed of eight precipitation cores (Fig. 2). Precipitation cores 2 and 3 were merged at 1648:30 LST. Precipitation core 4 was separated into two parts at 1717:30 (LST). The east and west parts were named precipitation core 4-1 and 4-2, respectively.

Figure 3 (a) shows the time-height distribution of the maximum reflectivity, top height of precipitation core and lightning initiation points in the target cell. Flash initiation points were divided into eight precipitation cores according to each area of a core observed every 30 sec. The core area is defined the square pole containing precipitation core. Extra 1km width outside the square pole was added to the core area. When the initiation point is located in an area of two precipitation cores, the core which have the nearest epicenter is selected. All of the top heights of precipitation cores abruptly increased in several minutes after the first detections except for the precipitation core 5. When the flash initiation points were ascended more than 10 km in height, the top heights of precipitation cores 2+3 and 4-1 were

* *Corresponding author address:* Yukie Moroda, National Institute for Information and Communications Technology, Koganei, Japan / Institute for Space-Earth Environment Research, Nagoya University, Nagoya, Japan; e-mail: ymoroda@rain.isee.nagoya-u.ac.jp

descended. Flash rate abruptly increased after 1648:00 LST (Fig. 3b). At this time, the top heights of PC2 and PC3 were elevated from 7 km to 10 km height within 6 minutes. The characteristics of the precipitation core and flashes are summarized in Table 1. In the precipitation cores 3, 4-1, and 7, the numbers of flashes were much more than precipitation cores 1, 5, and 6. While these cores with fewer flashes were characterized by higher CG flash rate. The number of precipitation cores 3 and 4-1 were included in the number of precipitation cores 2 and 4-2, respectively. Because these observation areas were mostly overlapped. An initiation point which identified at out of all the precipitation core areas is about 33 % as classified in OTHER in table 1.

Figure 4 shows longitude-height distribution of radar reflectivity at N34.95° and BOLT sources within 1 km from the latitude in the period from 1648:00 to 1659:30 LST. Precipitation cores 2 and 3 were merged at 1648:30. Then, the top height reached 10 km in height at 1650:30 LST. After that, the top height was descended with separating into many small fragments. Many fragments were descended with time, however, a fragment which identified at 1655:30 and located E 135.38° between 5 and 9 km heights was ascended (Figs. 4f, g, h). The fragment was ascended with weakening reflectivity. Additionally, around the fragments, many intracloud flashes occurred.

As shown in figure 5, many initiation points of IC flashes were located within 2 km from the top height of precipitation core. However, when the top height of precipitation cores 3, 4-1, and 7 descended, flash initiation points ascended. The color of flash initiation points indicates maximum reflectivity in the 1 km^3 region. These figures indicate that flashes which have the higher initiation points were occurred in the weaker reflectivity region. Figure 6 shows relationship between flash initiation heights and reflectivity. The initiation heights of IC flashes were inversely correlated with reflectivity with a slope of 0.17.

5. DISCUSSION AND SUMMARY

We studied the relationship between precipitation cores and lightning activity in the rapid development of the thunderstorm on 7 august 2015 using high temporal resolution data of PAWRs. When the two precipitation cores 2 and 3 were developed and were merged by strong updraft at lower level, the flash rate abruptly increased. Then, while the top height of precipitation core was maintained, many IC flashes occurred which initiation points were mainly within 2 km from the top height. After that, the top height was descended, because of attenuating precipitation core with weakened updraft at lower level. At the time, the precipitation cores were separated into several small fragments. Many of them descended, while a fragment showed upward motion with weakened reflectivity. Some IC flashes were occurred around top height of the ascending fragment. In the case of precipitation core 4-1, initiation points were more widely distributed vertically. These points were probably caused by ascending fragments separated from previously attenuated core in the precipitation core 4-2. The ascending fragments possibly consist of smaller graupel or ice crystals after the larger graupel or ice crystals fell down. Therefore, they were ascended by its buoyancy. In the period of attenuating precipitation core, 34 dBZ height was ascended from 11 to 14 km within 5 minutes. The intensity of reflectivity around flash initiation points were inversely proportional to the height. Ascending the initiation points were observed in the precipitation cores 3, 4-1, and 7, when these precipitation cores weakened. In the case of precipitation core 3, initiation points ascended two times during the period of 1648:30–1655:00 LST and 1655:00–1657:00 LST. The two ascent speeds of flash initiation points were 8.4 m s^{-1} and 15.1 m s^{-1}. The second ascending initiation points have a same speed as lightning bubble (Ushio et al., 2003). Most ascent speed of lightning bubbles are between 11 and 17 m s^{-1} (Ushio et al., 2003; Yoshida et al., 2016). Ascending fragment seems to be one of the causes of the lightning bubble. To clarify the characteristics of precipitation particles which are composed of ascending fragment, polarimetric radar observation data is believed to be useful. Additionally, what are characteristics of precipitation core to produce ascending fragments with IC flashes. This is the important future work.

5. REFERENCES

Cressman, G. P., 1959: An operational objective analysis system, Mon. Weather Rev., 87, 367-374.

Emersic, C., P. L. Heinselman, D. R. MacGorman, and E. C. Bruning, 2011: Lightning activity in a hail-producing storm observed with phased array radar, Mon. Weather Rev., 139, 1809-1825.

Shusse, Y., M. Maki, S. Shimizu, K. Iwanami, T. Maesaka, S. Suzuki, N. Sakurai, and R. Misumi, 2015: Relationship between precipitation core behavior in cumulonimbus clouds and surface rainfall intensity on 18 August 2011 in the Kanto Region. J. Meteor. Soc. Japan, 60, 967–977.

Takahashi, T., 1978: Riming electrification as a charge generation mechanism in thunderstorms, J. Atmos. Sci., 35, 1536–1548.

Ushio, T, S. J. Heckman, and H. J. hristian, 2003: Vertical development of lightning activity observed by the LDAR system: Lightning bubbles. J. Appl. Meteorol., 42, 165-174.

Yoshida, S, T. Wu, T. Ushio, K. Kusunoki, and Y. Nakamura, 2014: Initial results of LF sensor network for lightning observation and characteristics of lightning emission in LF band. J. Geophys. Res. Atmos., 119, 12,034-12,051.

Yoshida, S, T. Adachi, K. Kusunoki, S. Hayashi, T. Wu, T. Ushio, and E. Yoshikawa, 2017: Relationship between thunderstorm electrification and storm kinetics revealed by phased array weather radar. J. Geophys. Res. Atmos., 122, 3,821-3,836.

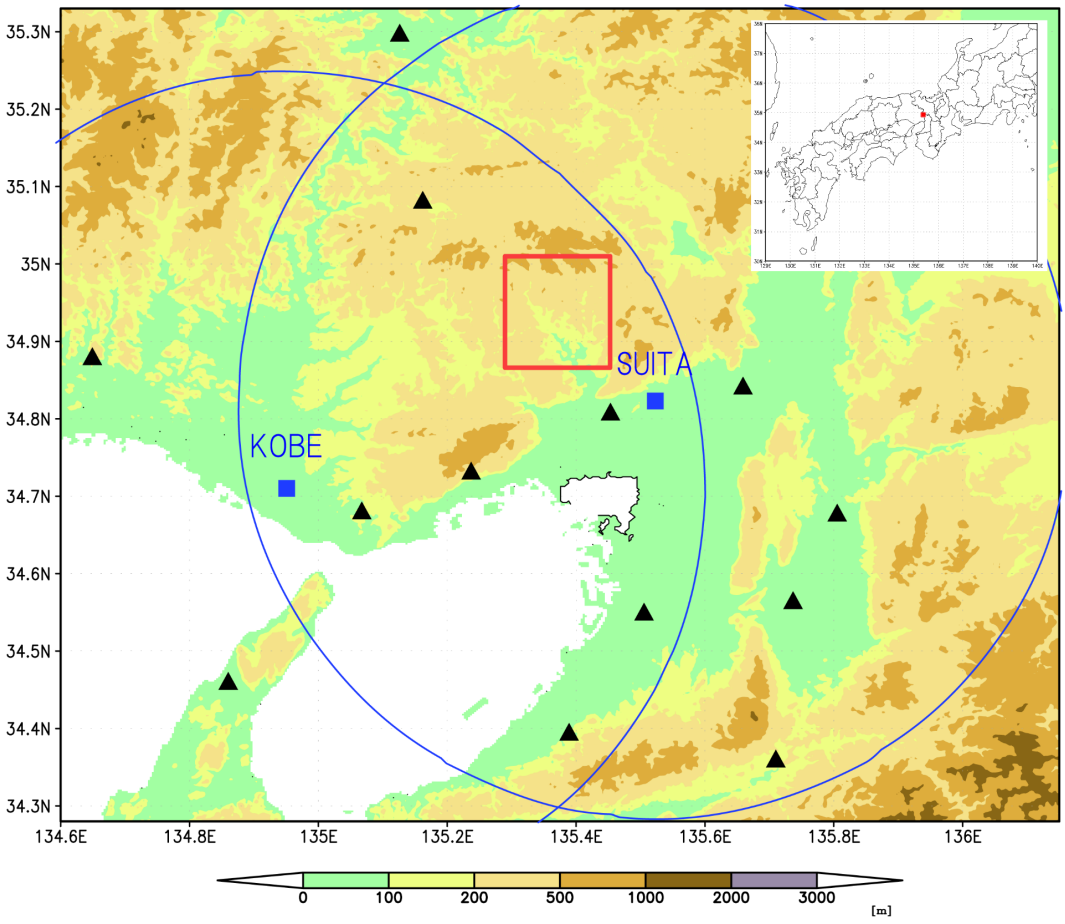

Fig. 1
Location of the PAWRs radar site (■) each covered a radius of 60 km (blue line), BOLT sensors (▲) and analysis domain (red square). The inset shows the location of the domain in large area.

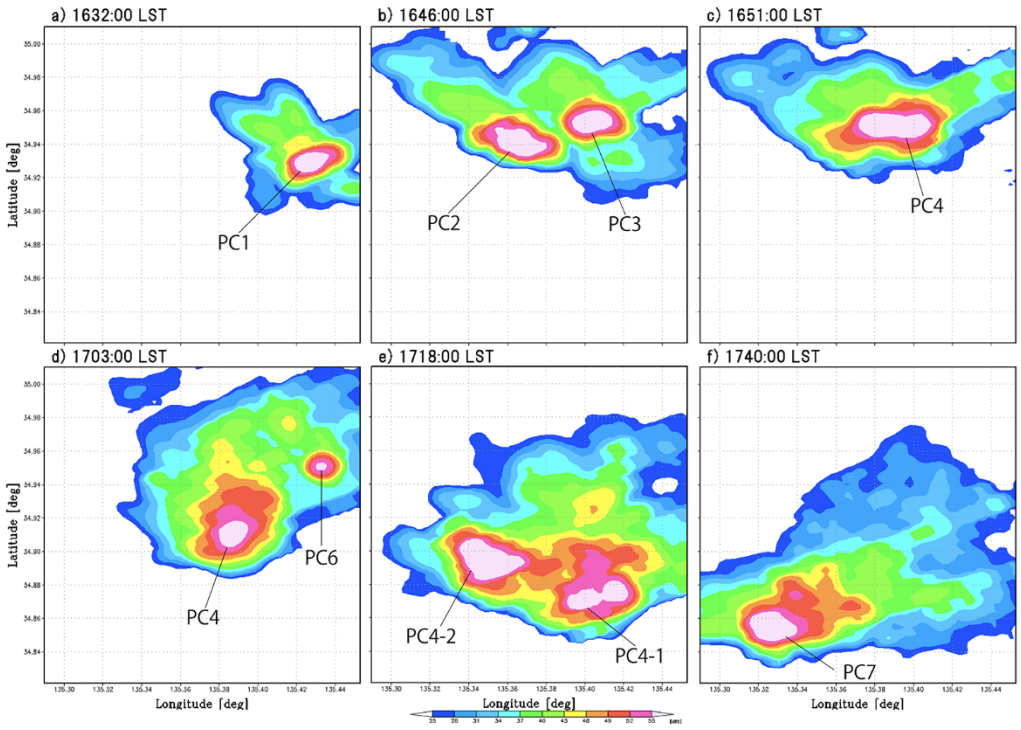

Fig. 2
Radar reflectivity at an altitude of 7 km data of the precipitation cell on 7 august 2015. All of the precipitation cores (P1, P2, P3, P4-1, P4-2, P7) were reached at this height except for precipitation core 5.

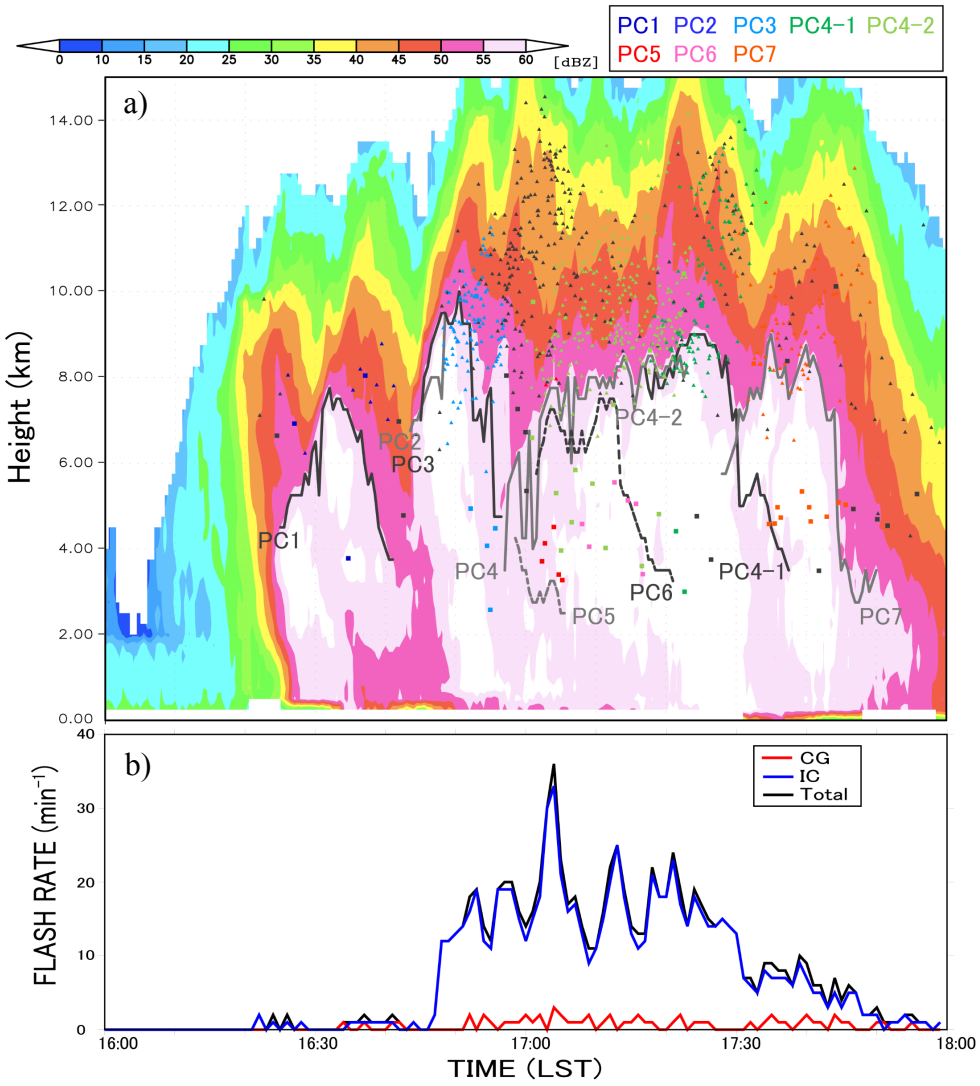

Fig. 3
Time-height distribution of maximum reflectivity in the target cell superimposed over top height of precipitation cores (black line or gray line) and flash initiation height (a). The triangles and squares correspond to the intracloud and cloud-to-ground flashes, respectively. Temporal change of the flash rate in the target cell (b). The blue and red line indicate intracloud and cloud-to-ground flashes, respectively.

Table 1
Characteristic of precipitation cores and flashes around each precipitation core.

Precipitation core						Flash			
Name	Lifetime of precipitation core (min)		Maximum top height (km)		Maximum volume (km3)	CG	IC	total	CG / total
PC1	16.5	(1625:00 – 1641:30)	7.75	(1632:00)	15.3	3	9	12	0.25
PC2	13.5	(1643:30 – 1657:00)	10.00	(1650:30)	45.3	–	–	–	–
PC3	12.0	(1645:00 – 1657:00)	10.00	(1650:30)	45.3	5	103	108	0.05
PC4_1	41.0	(1657:00 – 1738:00)	9.00	(1723:30)	85.1	16	347	363	0.04
PC4-2	26.5	(1657:00 – 1723:30)	8.50	(1714:00)	62.8	–	–	–	–
PC5	7.5	(1658:30 – 1706:00)	4.25	(1658:30)	4.4	5	2	7	0.71
PC6	20.0	(1701:30 – 1721:30)	7.50	(1710:30)	22.7	6	18	24	0.25
PC7	22.5	(1728:00 – 1750:30)	9.00	(1735:00)	34.3	11	72	83	0.13
OTHER	–	–	–	–	–	16	283	299	0.05

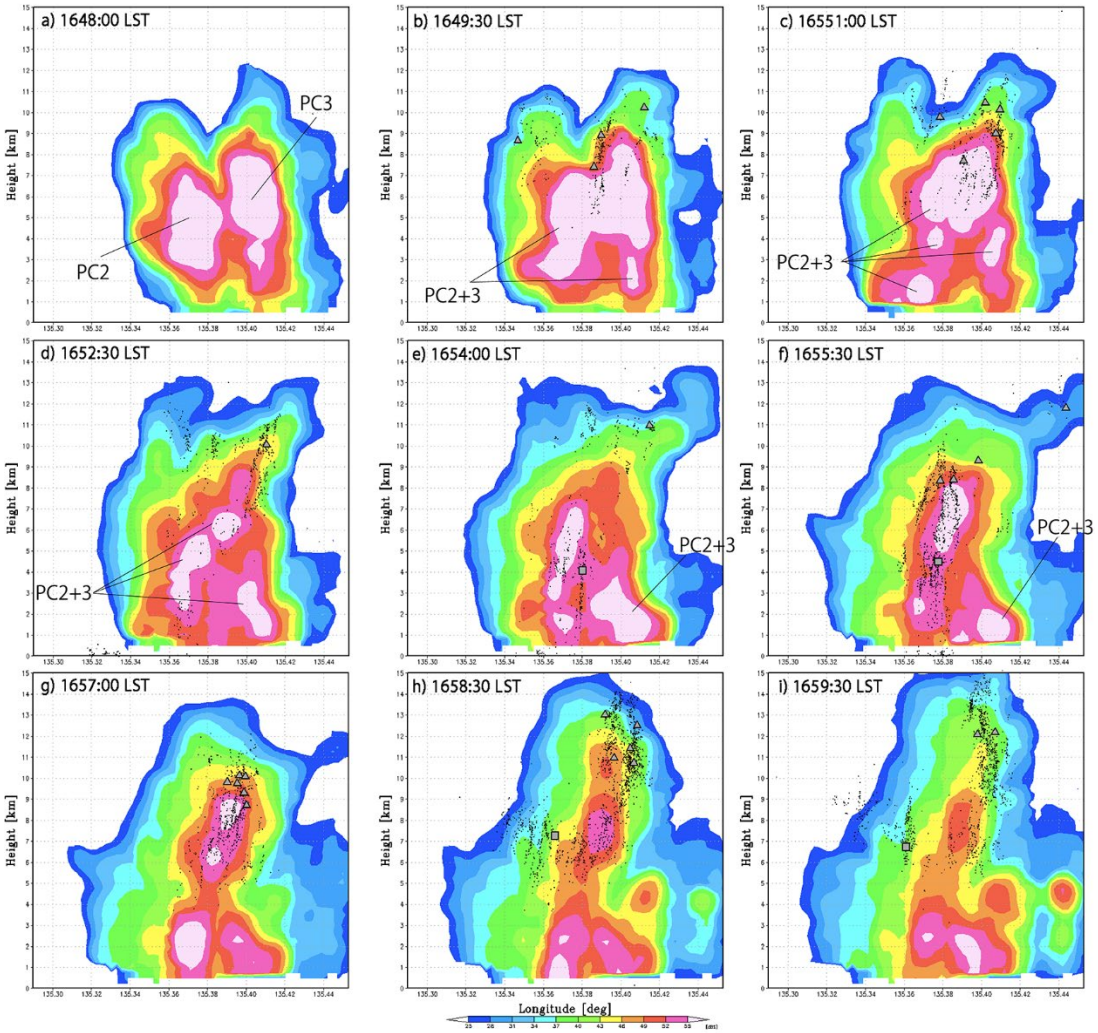

Fig. 4
Vertical cross section of reflectivity at N34.95° superimposed over BOLT sources from 1648:00 to 1650:30 LST. One or two volume scans data were skipped between each panel. The triangles and squares correspond to the intracloud and cloud-to-ground flashes, respectively.

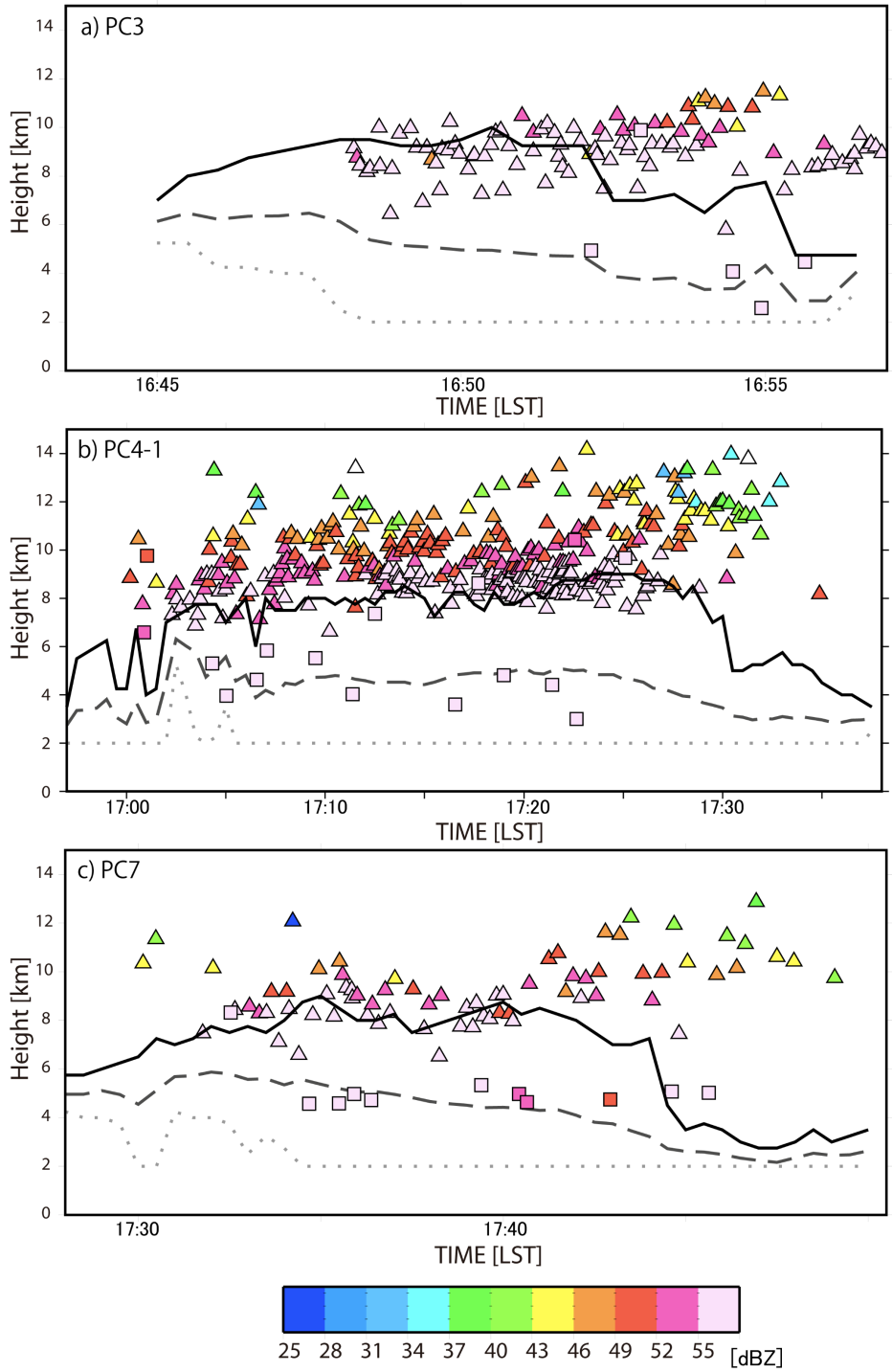

Fig. 5
Time evolution of top height (black line), epicenter (broken line), bottom height (dot line) of precipitation cores 3(a), 4-1(b), and 7 (c). Flash initiation height indicate the triangles and squares corresponded to the intracloud and cloud-to-ground flashes, respectively. The colored contour indicates the reflectivity at flash initiation points.

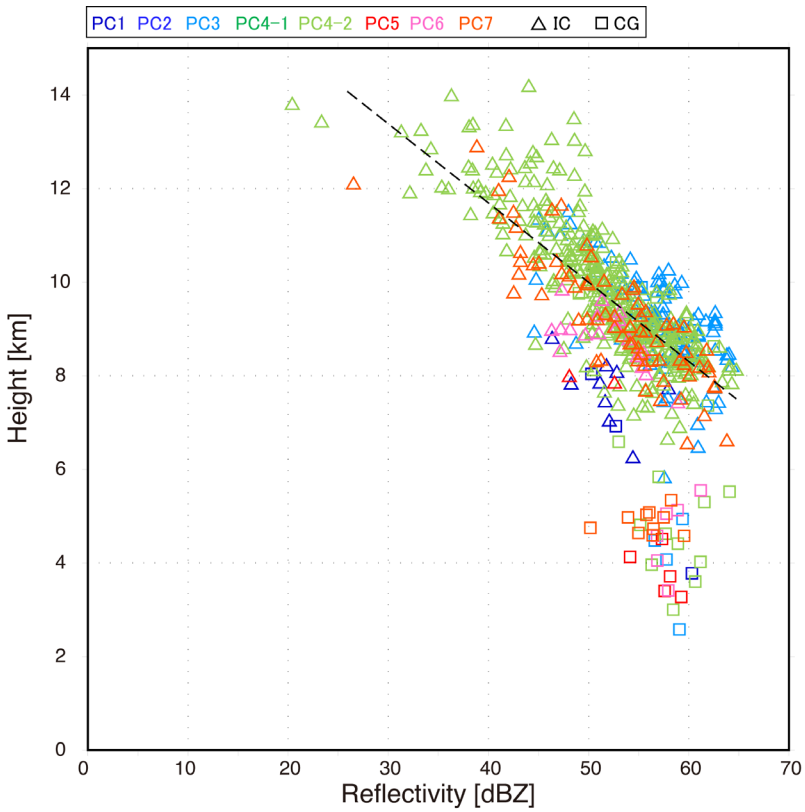

Fig. 6
Relationship between intensity of radar reflectivity and flash initiation height. Color indicate each precipitation core. The triangles and squares correspond to the intracloud and cloud-to-ground flashes, respectively.